ЯДЕРНА ФІЗИКА ТА ЕНЕРГЕТИКА / NUCL. PHYS. AT. ENERGY 24 (2023) 324-335 ISSN 1818-331X

ЯДЕРНА ФІЗИКА
NUCLEAR PHYSICS

УДК 539.142 https://doi.org/10.15407/jnpae2023.04.324

**K. Prathapan[1], M. K. Preethi Rajan[2], R. K. Biju[1,3,*]**

[1] *Department of Physics, Government Brennen College, Thallassery, India*
[2] *Department of Physics, Payyanur College, Payyanur, India*
[3] *Department of Physics, Pazhassi Raja NSS College, Mattanur, India*

*Corresponding author: bijurkn@gmail.com

# STUDY ON THE DECAY OF $Z$ = 127 – 132 SUPERHEAVY NUCLEI VIA EMISSION OF 1-N AND 2-N HALO NUCLEI

The barrier penetrability, decay constant and decay half-life of 1-n halo nuclei $^{11}$Be, $^{15,17,19}$C, $^{22}$N, $^{23}$O, $^{24,26}$F, $^{29,31}$Ne, $^{34,37}$Na, $^{35,37}$Mg, and $^{55}$Ca; and 2-n halo nuclei $^{22}$C, $^{27,29}$F, $^{34}$Ne, $^{36}$Na, and $^{46}$P from $Z$ = 127 – 132 parents were calculated within the framework of the Coulomb and proximity potential model by calculating the Q-values using the finite-range droplet model. A comparison between the decay half-lives is made by considering the halo candidates as a normal cluster and as a deformed structure with a rms radius. Neutron shell closure at 190, 196, 198, 200, 204, and 208 are identified from the plot of decay half-lives versus the neutron number of daughter nuclei ($N_P$). The calculation of alpha decay half-life and spontaneous decay half-life showed that the majority of the parent nuclei survive spontaneous fission and decay through alpha emission. The Geiger - Nuttall plots of $\log_{10} T_{1/2}$ versus $Q^{-1/2}$ and universal plots of $\log_{10} T_{1/2}$ versus $-\ln P$ for the emission of all 1-n and 2-n halo nuclei from the parents considered here are linear and show the validity of Geiger - Nuttall law in the case of decay of halo nuclei from superheavy elements.

*Keywords:* cluster radioactivity, halo nuclei, superheavy elements.

## 1. Introduction

A halo is a weakly bound nuclear system in which the last one or two nucleons remain beyond the interaction potential of the nucleus and hence possess a much larger matter radius than a normal nucleus [1, 2]. For such nucleons, the separation energy is extremely small, usually of the order of 1 MeV or even less. The halo can be either a neutron halo or a proton halo [3, 4]. The existence of a halo was first identified in $^{11}$Li nuclei in 1985 by Tanihata et al [5]. The existence of a halo in $^{11}$Li, $^{11}$Be, $^{14}$Be, $^{14}$B, $^{15}$C, and $^{19}$C was experimentally confirmed in the laboratory [6]. Other proposed candidates for neutron halo include $^{6,8}$He, $^{12}$Be, $^{17,19}$B, $^{17,22}$C, $^{22}$N, $^{23}$O, $^{24,26,27,29}$F, and $^{29}$Ne [2, 7]. The first experimentally produced neutron halo nucleus is $^{6}$He [8]. After the introduction of radioactive beam facilities, studies on the structure and other properties of halo nuclei became more popular among nuclear scientists [9 - 13].

The shell model and mean field approaches cannot be used successfully for describing the halo structure of a nucleus [14]. The reaction cross-section measurements are widely used to obtain information about the existence and structure of halo nuclei [15 - 18]. In 2009, by measuring the reaction cross-sections for single-neutron removal from the very neutron-rich nucleus $^{31}$Ne on lead and carbon targets at an energy of 230 MeV per nucleon using the RIBF facility at RIKEN, T. Nakamura et al. predicted the halo structure of $^{31}$Ne nucleus as s- or p-orbital halo [19]. In 2014, Takechi et. al. confirmed the existence of a $^{37}$Mg halo nucleus through the measurement of reaction cross-section [20].

Apart from the large matter radius, halo nuclei exhibit new magic numbers resulting from the dynamic effects of nucleon-nucleon interaction. The emergence of new magic numbers can be predicted through the study of the stability of parent nuclei against alpha decay and by using relativistic mean-field calculations [21, 22]. To study the structure and formation of halo nuclei, many structural models that include two-body systems, three-body systems, and microscopic models as well as many reaction models are available [23 - 26].

In the present work, our aim is to study the possibility of the emission of 1- and 2-neutron halo nuclei from parents with $Z$ = 127 – 132, in the superheavy region. The studies on the synthesis of superheavy elements became more popular after the establishment of experimental facilities for hot fusion reactions at JINR-FLNR (Russia) and at GSI (Germany), and cold fusion reactions at RIKEN (Japan) [27 - 32]. Superheavy elements with $Z$ = 112 – 118 were successfully synthesized through various fusion reactions with a $^{48}$Ca beam on various actinide targets at FLNR (Dubna), GSI (Darmstadt), and LBNL (Berkeley) [33]. The last element that was successfully synthesized is Oganesson ($Z$ = 118, $A$ = 294) through the 3n-evaporation channel of the $^{249}Cf + {}^{48}Ca$ reaction [34]. Recently, many theoretical and experimental studies have been conducted on the synthesis of $Z$ = 119 and 120 nuclei [35 - 38]. In 2014, Zhu et al., studied the reaction cross-sections based on $^{48}Ca + {}^{252}Es$, $^{50}Ti + {}^{249}Bk$, and $^{51}V + {}^{248}Cm$ fusion reactions for the synthesis of $Z$ = 119 and 120 nuclei [39]. Many experimental attempts were also made to synthesize these elements [33, 40, 41]. The experimental studies on the synthesis of elements with $Z$ = 119 and higher through hot fusion reactions require highly intense beams and improved detection facilities. In 2016, Santhosh et al. studied the different decay modes of $Z = 104 - 136$ even-even nuclei [42]. Our study is motivated by the synthesis of superheavy elements by fusion reactions and the prediction of the existence of elements with higher atomic numbers such as 124, 126, and 128 [43 - 45]. We would like to point out that we have already made an attempt to study the formation of proton halo nuclei from superheavy elements and the results were published [46, 47].

In Section 2, the details of the model used for the study are discussed. In Section 3, the results of our calculations are given.

## 2. The Coulomb and proximity potential model

For our study, we have used the Coulomb and proximity potential model (CPPM), which is one of the most successful models used to describe the decay of heavy fragments from elements in heavy and superheavy regions. This model assumes the interaction potential barrier as the sum of Coulomb, proximity, and centrifugal potentials for the touching configuration and for the separated fragments [48]. For the overlap region, a simple power law interpolation provided by Shi and Swiatecki [49] is used. The introduction of proximity potential makes the barrier more realistic and reduces the height of the barrier. Also, the results of calculations obtained through this model are closely in agreement with the experimental data. For a parent nucleus exhibiting exotic decay, the interacting potential barrier can be written as

$$V = \frac{Z_1 Z_2 e^2}{r} + V_p(z) + \frac{\hbar^2 l(l+1)}{2\mu r^2}; \text{ for } z > 0. \quad (1)$$

In the above expression, $Z_1$ and $Z_2$ are the atomic numbers of the daughter and the emitted cluster, $z$ is the distance between the near surface of the fragments, $r$ is the distance between the fragment centres, which is given as $r = z + C_1 + C_2$. The quantity $l$ is the angular momentum quantum number, $\mu$ is the reduced mass and $V_p(z)$ is the proximity potential. The proximity potential is given by Blocki et al. [50] as

$$V_p(z) = 4\pi\gamma b\left[\frac{C_1 C_2}{(C_1 + C_2)}\right]\Phi\left(\frac{z}{b}\right), \quad (2)$$

where $\gamma$ is the nuclear surface tension coefficient, $b$ is the width of the nuclear surface (diffuseness), $C_i$ are Süssmann central radii and $\Phi$ the universal proximity potential. These equations are applied to spherical nuclei.

The nuclear surface tension coefficient [48] is given by

$$\gamma = 0.9517\left[1 - 1.7826(N - Z)^2 / A^2\right] \text{ MeV/fm}^2, \quad (3)$$

where $N, Z$ and $A$ represents the neutron number, proton number and mass number of the nucleus. The universal proximity potential [50] is given by the expression

$$\Phi(\varepsilon) = -4.41 e^{-\varepsilon/0.7176}, \text{ for } \varepsilon \geq 1.9475 \quad (4)$$

and

$$\Phi(\varepsilon) = -1.7817 + 0.9270\varepsilon + 0.0169\varepsilon^2 - 0.05148\varepsilon^3,$$

$$\text{for } 0 \leq \varepsilon \leq 1.9475, \quad (5)$$

where $\varepsilon = (z/b)$ with $b \approx 1$. The Süssmann central radii $C_i$ of fragments are related to the sharp radii $R_i$ as

$$C_i = R_i - \left(\frac{b^2}{R_i}\right). \quad (6)$$

The sharp radii $R_i$ can be calculated by using an empirical formula in terms of the mass numbers $A_i$ as [51]

$$R_i = 1.28 A_i^{1/3} - 0.76 + 0.8 A_i^{-1/3}. \quad (7)$$

The potential for the overlap region of the barrier is given as

$$V = a_0 (L - L_0)^n, \text{ for } z < 0. \quad (8)$$

In this expression, $L = z + 2C_1 + 2C_2$ and $L_0 = 2C.$ The constant $a_0$ and the parameter $n$ are determined by the smooth matching of the two potentials at the touching point.

The barrier penetrability $P$ can be obtained by using one-dimensional WKB approximation and is given as

$$P = \exp\left\{-\frac{2}{\hbar}\int_a^b \sqrt{2\mu(V-Q)}dz\right\}, \qquad (9)$$

where $a$ and $b$ are the turning points given by $V(a) = V(b) = Q$ and $Q$ is the energy released in the decay process.

Also $\mu = mA_1A_2/A$ is the reduced mass with $A_1$ and $A_2$ are the mass numbers of the emitted daughter and cluster nuclei respectively. This integral can be evaluated numerically or analytically to get the half-life time of decay as

$$T_{1/2} = \frac{\ln 2}{\lambda} = \frac{\ln 2}{\nu P}, \qquad (10)$$

where $\nu = \frac{\omega}{2\pi} = \frac{2E_V}{h}$ is the number of assaults on the barrier per second assuming a harmonic motion and $E_V$ is the zero-point vibration energy and is given by the empirical formula of Poenaru et al. [52] as

$$E_V = Q\left\{0.056 + 0.039\exp\left[\frac{(4-A_2)}{2.5}\right]\right\}, \text{ for } A_2 \geq 4. \qquad (11)$$

The zero-point vibration energy $E_V$ vary only slightly with the mass $A_2$ of the cluster. This helps to predict the decay half-life with high accuracy [52].

## 3. Results and discussion

The barrier penetrability, decay constant, and the half-life of decay of 1-n and 2-n halo nuclei from $Z = 127 - 132$ were calculated using the CPPM. The CPPM is a well-established model and has been extensively used by Santhosh et al., during the past decade [53 - 58]. The model can accurately predict the alpha decay chains, heavy particle decays from elements in heavy and superheavy regions; and the predictions are in good agreement with other models such as the universal (UNIV) curve of Poenaru et al. [59], universal decay law, the analytical formula of Royer [60], Viola - Seaborg - Sobiczewski semi-empirical relation [61], Gamow-like model of Zdeb et al. [62] and semiempirical relation of Hatsukawa et al. [63]. We would like to point out that we have already used the CPPM for studying the emission of 1-p and 2-halo nuclei [46, 47] and to study the emission of various exotic nuclei from superheavy elements [64, 65].

The possibility for the existence of a neutron halo structure in a nucleus can be identified by calculating the 1-n and 2-n separation energies. For a 1-n halo, 1-n separation energy is the lowest and less than 1 MeV, and for a 2-n halo nucleus, its 2-n separation energy will be the lowest and less than 1 MeV. To confirm the halo structure, we have calculated the driving potential [48] for halo nuclei with $Z = 11 - 20$, and the halo nuclei with $Z = 3 - 10$ are directly taken from the work of Santhosh et al. [66], where detailed calculation of driving potentials is given. The possible 1-n halo candidates in the selected range are $^{11}$Be, $^{14}$B, $^{15,17,19}$C, $^{22}$N, $^{23}$O, $^{24,26}$F, $^{29,31}$Ne, $^{34,37}$Na, $^{35,37}$Mg, and $^{55}$Ca. The 2-n halo candidates are $^{6,8}$He, $^{11}$Li, $^{12,14}$Be, $^{17,19}$B, $^{22}$C, $^{27,29}$F, $^{34}$Ne, $^{36}$Na, and $^{46}$P. In the present work, we have studied the possibility of the emission of these halo nuclei from elements with $Z = 127 - 132$.

The emission of a halo nucleus from a parent is possible only if the Q-value for the decay process is positive. The Q-value is calculated using the expression

$$Q = M(A,Z) - M(A_1,Z_1) - $$
$$-M(A_2,Z_2) + k\left(Z^{\varepsilon}_{A,Z} - Z^{\varepsilon}_{A_1,Z_1}\right). \qquad (12)$$

In this expression, $M(A,Z)$, $M(A_1,Z_1)$ and $M(A_2,Z_2)$ represent the mass excess of the parent, daughter, and emitted halo nucleus respectively, and the term $k\left(Z^{\varepsilon}_{A,Z} - Z^{\varepsilon}_{A_1,Z_1}\right)$ accounts for the screening effect of the atomic electrons [67]. For nuclei with $Z \geq 60$, $k = 8.7$ eV and $\varepsilon = 2.517$. For nuclei $Z < 60$, they are 13.6 eV and 2.408 respectively [68]. The experimental mass excess values of halo nuclei are taken from the tables of Koura - Tachibana - Uno - Yamada [69]. The mass excess values of the superheavy elements are taken from the atomic data tables of Möller et al. [70] where the mass excess value calculations are based on the finite-range droplet macroscopic model.

For light halo nuclei such as $^{6,8}$He, $^{11}$Li, $^{12,14}$Be, and $^{14}$B, the mass excess values are high, and the Q-value of their decay is very small or even negative. From the isotopes of the parents $Z = 127 - 132$, the barrier penetrability and half-life for the emission of 1-n halo nuclei $^{11}$Be, $^{15,17,19}$C, $^{22}$N, $^{23}$O, $^{24,26}$F, $^{29,31}$Ne, $^{34,37}$Na, $^{35,37}$Mg, and $^{55}$Ca; and 2-n halo nuclei $^{22}$C, $^{27,29}$F, $^{34}$Ne, $^{36}$Na, and $^{46}$P were determined using CPPM. For many of the halo nuclei considered here, the half-life of decay is found to be far above the experimental limit. Only for $^{11}$Be, $^{15,17}$C, $^{23}$O, $^{24,26}$F, $^{29}$Ne, and $^{35}$Mg the half-life of decay is found to be less than or slightly above the experimental limit for the emission from the $Z = 127 - 132$ parents. We have calculated the decay half-life for zero momentum transfers since the angular momentum transferred in the process is extremely small $(\approx 5\hbar)$ and can be neglected. The results of our calculation and more detailed discussions are given in the following paragraphs.

Since the halo is a highly deformed nuclear state, the expression for radius $R_i = R_0 A_i^{1/3}$ cannot represent the structure of the halo nuclei completely. To some extent the surface effects are included in the Süssmann central radii $(C_i)$; however, $R_i$ is a function of $A_i$ alone. Therefore, we have considered the concept of rms radius of the halo nucleus. For a deformed halo structure, the rms radius is found to be larger than its normal radius. For our calculation purpose, the rms radius for halo nuclei $Z \le 10$ is directly taken from reference [7] and for $Z$ = 11 – 20, we have calculated using the expression [71]:

$$\langle R_i \rangle = \langle R_i \rangle_{sph} \left(1 + \frac{5}{4\pi} \langle \beta_2^2 \rangle \right)^{1/2}, \qquad (13)$$

where $\langle R_i \rangle_{sph}$ is the spherical radius of the halo nucleus given by $R_0 A_i^{1/3}$ and $\beta_2$ is the quadrupole deformation. The $\beta_2$ values are taken from reference [70]. We have considered about 2653 possible decays of the 1-n and 2-n halo nuclei from the isotopes of $Z = 127 – 132$ parents. It is to be mentioned that most of the parent nuclei are stable against the decay of 1-n and 2-n halo nuclei; however, we could find some decays that are possible with a decay half-life well within the experimental limit. Such results are given in Table. For other 1-n halo nuclei, $^{14}$B, $^{17,19}$C, $^{22}$N, $^{26}$F, $^{29,31}$Ne, $^{34,37}$Na, $^{35,37}$Mg, and $^{55}$Ca and 2-n halo nuclei $^{6,8}$He, $^{11}$Li, $^{12,14}$Be, $^{17,19}$B, $^{22}$C, $^{27,29}$F, $^{34}$Ne, $^{36}$Na, and $^{46}$P, the half-life of decays are very much above the experimental limit.

**The predicted half-lives for the emission of different neutron halo nuclei from various isotopes of $Z$ = 127 – 132 nuclei by considering the emitted nuclei as clusters and as halo**

| Parent nuclei | Emitted halo nuclei | Q-value, MeV | Barrier penetrability, P | | Decay constant, λ | | $\log_{10}T_{1/2}$, s | |
|---|---|---|---|---|---|---|---|---|
| | | | Normal cluster | Halo | Normal cluster | Halo | Normal cluster | Halo |
| $^{332}$129 | $^{11}$Be | 20.96 | $2.011\cdot10^{-49}$ | $3.810\cdot10^{-45}$ | $1.303\cdot10^{-28}$ | $2.469\cdot10^{-24}$ | 27.725 | 23.448 |
| $^{333}$130 | $^{11}$Be | 21.64 | $4.555\cdot10^{-48}$ | $8.939\cdot10^{-44}$ | $3.040\cdot10^{-27}$ | $5.965\cdot10^{-23}$ | 26.357 | 22.065 |
| $^{334}$130 | $^{11}$Be | 20.67 | $3.908\cdot10^{-5}$ | $7.474\cdot10^{-47}$ | $2.501\cdot10^{-30}$ | $4.783\cdot10^{-26}$ | 29.442 | 25.161 |
| $^{335}$130 | $^{11}$Be | 22.39 | $9.835\cdot10^{-46}$ | $1.916\cdot10^{-41}$ | $6.772\cdot10^{-25}$ | $1.319\cdot10^{-20}$ | 24.010 | 19.720 |
| $^{336}$130 | $^{11}$Be | 21.33 | $6.070\cdot10^{-49}$ | $1.159\cdot10^{-44}$ | $3.997\cdot10^{-28}$ | $7.639\cdot10^{-24}$ | 27.238 | 22.957 |
| $^{335}$131 | $^{11}$Be | 21.27 | $5.498\cdot10^{-50}$ | $1.089\cdot10^{-45}$ | $3.612\cdot10^{-29}$ | $7.157\cdot10^{-25}$ | 28.283 | 23.986 |
| $^{336}$131 | $^{11}$Be | 22.62 | $8.128\cdot10^{-46}$ | $1.636\cdot10^{-41}$ | $5.649\cdot10^{-25}$ | $1.137\cdot10^{-20}$ | 24.008 | 19.784 |
| $^{337}$131 | $^{11}$Be | 21.95 | $8.524\cdot10^{-48}$ | $1.685\cdot10^{-43}$ | $5.763\cdot10^{-25}$ | $1.139\cdot10^{-22}$ | 26.080 | 21.783 |
| $^{337}$132 | $^{11}$Be | 23.47 | $4.045\cdot10^{-44}$ | $8.377\cdot10^{-40}$ | $2.908\cdot10^{-23}$ | $6.023\cdot10^{-19}$ | 22.377 | 18.061 |
| $^{338}$132 | $^{11}$Be | 22.46 | $5.070\cdot10^{-47}$ | $1.035\cdot10^{-42}$ | $3.501\cdot10^{-26}$ | $7.148\cdot10^{-22}$ | 25.296 | 20.986 |
| $^{329}$128 | $^{23}$O | 61.96 | $6.953\cdot10^{-52}$ | $4.137\cdot10^{-47}$ | $1.167\cdot10^{-29}$ | $7.168\cdot10^{-26}$ | 28.733 | 24.985 |
| $^{337}$132 | $^{23}$O | 64.43 | $7.301\cdot10^{-52}$ | $3.906\cdot10^{-47}$ | $1.314\cdot10^{-30}$ | $7.030\cdot10^{-26}$ | 29.722 | 24.993 |

We have calculated the half-life of decay of the halo nuclei by considering them as a normal spherical cluster and as a deformed nucleus with a rms radius. Figs. 1 and 2 represent the results of our calculations; the logarithmic value of half-life is plotted against the neutron number of daughter nuclei ($N_d$). A peak in the plot represents the neutron shell closure of the parent nucleus and a dip represents the neutron shell closure of the daughter nucleus. In the Figures we have included $^{11}$Be and $^{23}$O only; for other halo nuclei, the decay half-lives are larger than the experimental upper limit.

Fig. 1 is the plot of $\log_{10} T_{1/2}$ versus the neutron number of daughter nuclei ($N_d$) and shows the comparison of decay half-lives of $^{11}$Be from the isotopes of $Z$ = 127 – 132 parent nuclei when it is considered as a normal spherical cluster and as a deformed halo nucleus. It can be seen that the half-life of decay is lower for the halo structure than for the normal cluster. From $Z$ = 129, 130, 131, and 132 parents $^{11}$Be has shown finite probability for the emission with a half-life of less than $10^{30}$ s. Also, the plots in Fig. 1 show dips at daughter neutron numbers 190, 196, and 198, which represent the shell closure of daughter nuclei at these neutron numbers. Also, the prominent peaks at $N_d$ = 193 in Fig. 1, *a* and *b* show the stability of the parent nuclei against the decay. At these peaks, the parents have a neutron number of 200 and the stability of the parent at these neutron numbers is due to the neutron shell closure of the parent. In Fig. 1, *c*, the peak at $N_d$ = 183 represents the stability of the parent which has a neutron number $N_p$ = 190; and the peak at $N_d$ = 193 corresponds to $N_p$ = 200. This shows that the neutron shell closure of the parent nuclei occurs at 190 and 200. In Fig. 1, *d*, there is a peak at $N_d$ = 183 which corresponds to $N_p$ = 190, and a second peak at $N_d$ = 201, which corresponds to $N_p$ = 208. Therefore, neutron shell closure of the parents occurs at these neutron numbers. Therefore, at neutron numbers 190, 196, 198, 200, and 208 the nucleus possesses a stable configuration due to neutron shell closure.

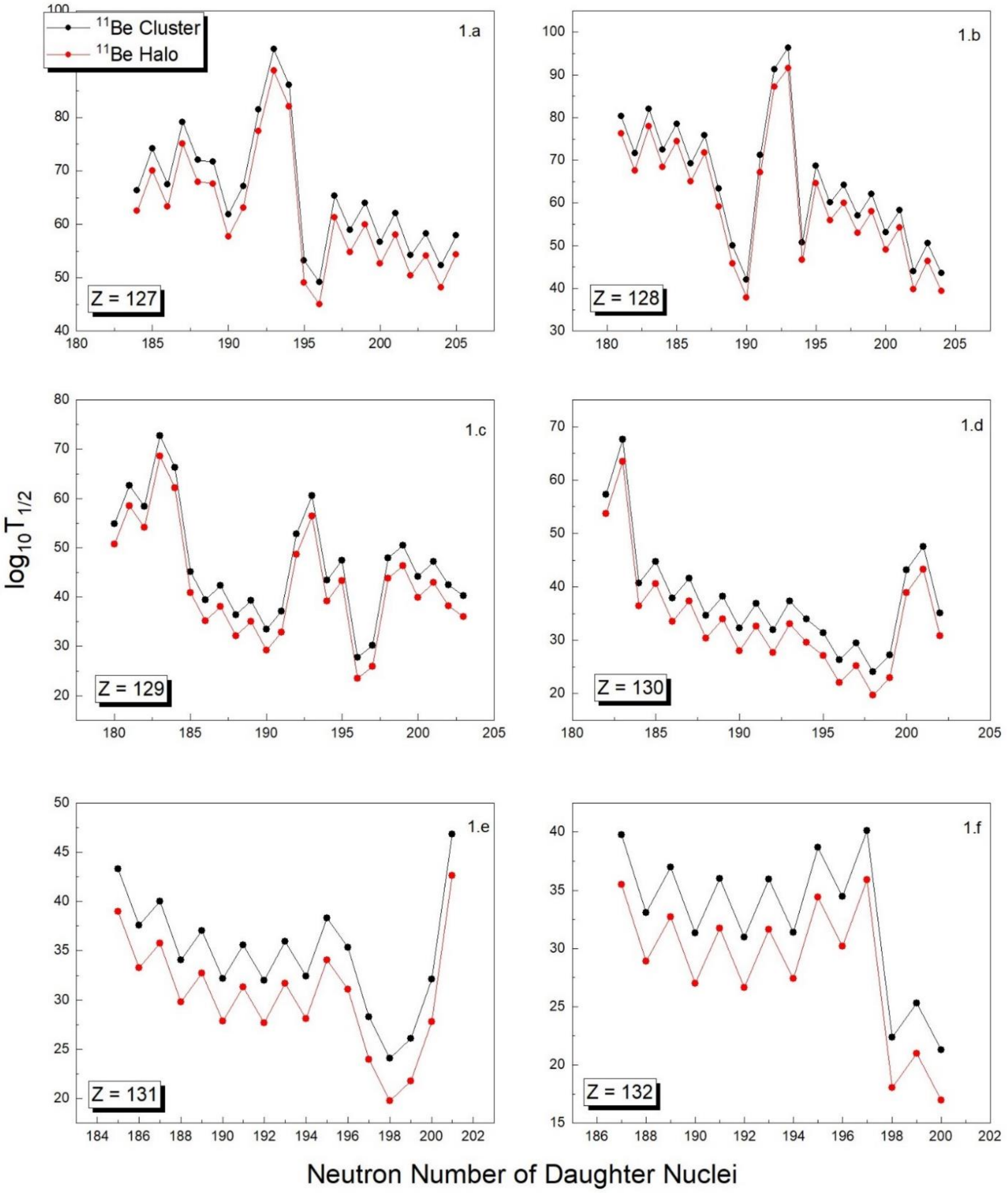


Fig. 1. Comparison of the half-life of emission of $^{11}$Be halo nucleus from $Z = 127 - 132$ superheavy elements as a spherical cluster and as a deformed nucleus with rms radius. (See color Figure on the journal website.)

The comparison of decay half-lives of the $^{23}$O nucleus as a cluster and as a halo from the selected parents is given in Fig. 2. In this case, also it is observed that the decay half-life decreases when the rms radius is considered. In plots 2, *a*, *b* and *c*, there are peaks at $N_d = 185$, all corresponding to stable parents with neutron number $N_p = 200$. This again confirms the neutron shell closure at a neutron number 200, providing additional stability to the nucleus. Further, in Fig. 2, *a*, there is a dip $N_d = 188$ and in Fig. 2, *f*, there is a dip at $N_d = 190$, which indicates that the daughter nuclei formed in this case are stable at these neutron numbers.

For the emission of $^{24}$F from the $Z = 127 - 132$ isotopes, the decay half-life is decreased when the rms radius of the halo structure is considered. However, we could find dominant peaks at $N_d = 185$ only for $Z = 128$ and 129 corresponding to a parent neutron number $N_p = 200$. Further, the emission of $^{24}$F from the selected parents is less probable than $^{11}$Be and $^{23}$O.

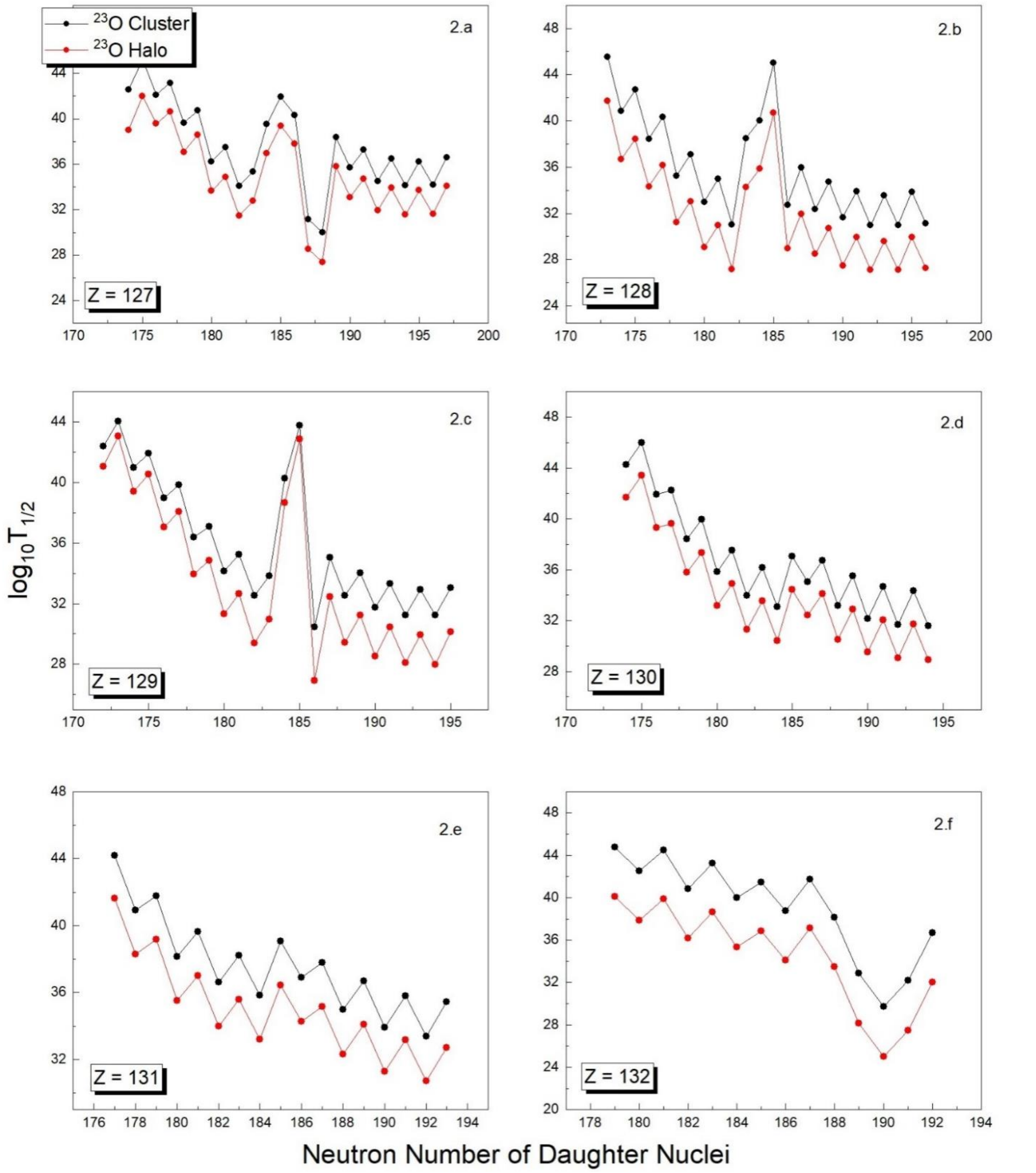


Fig. 2. Comparison of the half-life of emission of $^{23}$O halo nucleus from $Z$ = 127 – 132 superheavy elements as a spherical cluster and as a deformed nucleus with rms radius. (See color Figure on the journal website.)

The prominent peaks in the plots correspond to a parent neutron number $N_p = 200$ indicating the exemptional stability of the nucleus and we predict that 200 is a neutron magic number. It is to be mentioned that calculations based on Weizsäcker - Skyrme model and finite-range droplet model have already predicted neutron shell closure at 196, 198, 200, and 202 [72]. For the other halo nuclei considered here, even the minimum decay half-life is near and far above the experimental limit. So, such plots are not included here. However, it is to be mentioned that in the case of other halo nuclei, the decay half-life is decreased when the rms radius of the halo structure is considered. Further, in Figs. 1 and 2, one can observe an odd-even staggering in the plots of neutron number versus the logarithmic value of decay half-lives. This is due to the odd nucleon blocking effect where the odd nucleon hinders the preformation of the cluster and thereby causes an increase in the decay half-life compared to that of neighbouring isotopes.

To confirm the feasibility of our study, we have made a calculation of the spontaneous fission half-life and alpha decay half-life of the parent nuclei $Z = 127 - 132$. The spontaneous fission half-lives were calculated using the formula of C. Xu et al. [73] given by

$$T_{1/2} = \exp\left\{2\pi\left[\begin{matrix} c_0 + c_1 A + c_2 Z^2 + c_3 Z^4 + c_4 \left(N - Z\right)^2 \\ -\left(0.13323\dfrac{Z^2}{A^{1/3}} - 11.64\right) \end{matrix}\right]\right\}, \tag{14}$$

where the half-life is in years, $A$ – is the mass number, and $Z$ – is the atomic number of the parent nucleus. The values of the constants $c_1, c_2, c_3,\ c_4$ are taken from the Ref. [73]. The alpha decay half-lives were calculated using the Viola - Seaborg semi-empirical relationship given by [61]

$$\log_{10} T_{1/2} = \left(aZ + b\right)Q^{-1/2} + cZ + d + h_{\log}, \tag{15}$$

where the half-life is in seconds, the Q-value is in MeV and $Z$ is the atomic number of a parent nucleus. The values of the constants *a, b, c, d*, and $h_{\log}$ are taken from Ref. [74]. The alpha decay half-lives were also calculated using the Universal Decay Law of Qi et al. [75] given by

$$\log_{10} T_{1/2} = aZ_c Z_d \sqrt{\frac{A}{Q_c}} + b\sqrt{AZ_c Z_d \left(A_c^{1/3} + A_d^{1/3}\right)} + c, \tag{16}$$

where $A = \dfrac{A_c A_d}{A_c + A_d}$ the constants, $a$ = 0.4065, $b$ = –0.4311, and $c$ = –20.7889 are the coefficient sets determined by fitting to experiments of alpha decays [75].

The results of our calculations are shown in Fig. 3; the half-lives of spontaneous fission and alpha decay are plotted against the mass number of the parent nuclei. The half-lives of halo emission against the mass number of parent nuclei are also plotted in the same Figure. From the plot, it is clear that the spontaneous fission half-lives of the majority of the parent nuclei are much larger than their alpha decay half-life and hence they decay through alpha emission. The $Z = 127$, the isotopes with $A > 333$ decay via spontaneous fission and $Z = 128$, isotopes with $A > 337$ decay via spontaneous fission. The isotopes of parent nuclei with $Z$ = 129, 130, 131, and 132 decay via alpha emission. Similar predictions can be found in references [42] and [55]. Theoretical calculations show that the heaviest elements decay by alpha emission [76] and are experimentally verified up to $^{294}$118 [77]. At present, the lower limit of decay half-life for the experimental detection is ~ $10^{-6}$ s [77 - 79]. From Fig. 3 it is clear that the decay half-lives for halo nuclei $^{11}$Be, $^{23}$O, and $^{24}$F from $Z = 127 - 132$ are less than the SF half-lives and are also lower than the experimental upper limit of $10^{30}$ s; so, these clusters can be detected in experiments. The gas-filled separators (at FLNR, RIKEN, and GSI), velocity filters (at GSI and GANIL), and the multi-reflection time-of-flight mass spectrograph, MRTOF-MS (at ISOLDE, RIKEN, GANIL, and TRIUMF) are widely used in the detection of short-lived superheavy nuclei [79, 80]. The existing experimental setups are sensitive for nuclei with half-lives roughly between tens of μs up to a few hours [81]. Recently a "$\alpha$-TOF'' detector with a time resolution of 250.6 ± 6.8 ps was developed for correlated measurement of atomic masses and decay properties of superheavy elements [82, 83].

Now, to confirm the validity of the CPPM for applying to study the decay of halo from superheavy elements, we have plotted the Geiger - Nuttall plots (G-N) for all the 1-n and 2-n candidates considered here. Even though the G-N law is originally used to explain the alpha decay process [84] assuming Coulomb interaction, it can be applied for cluster radioactivity also [85 - 89]. Thus, we expect that the linearity of the G-N plot will not be affected by the introduction of the proximity potential along with Coulomb interaction. According to the G-N law, the logarithmic value of decay half-life follows a linear relationship with $Q^{-1/2}$ as per the equation

$$\log_{10} T_{1/2} = MQ^{-1/2} + C, \tag{17}$$

where $M$ is the slope of the curve and $C$ is the y-intercept.

Fig. 4 shows the G-N plot of 1-n and 2-n halo nuclei for the decay from the isotopes of $Z = 127$ parent nuclei. It is clear that all the plots are linear without any discontinuity. This indicates that the linearity of the plot is not altered much by the introduction of the proximity potential and confirms the validity of the G-N plot for the decay of halo nuclei. For the emission from other parents with $Z = 128 - 132$, we obtained similar linear plots; however, they are not included here.

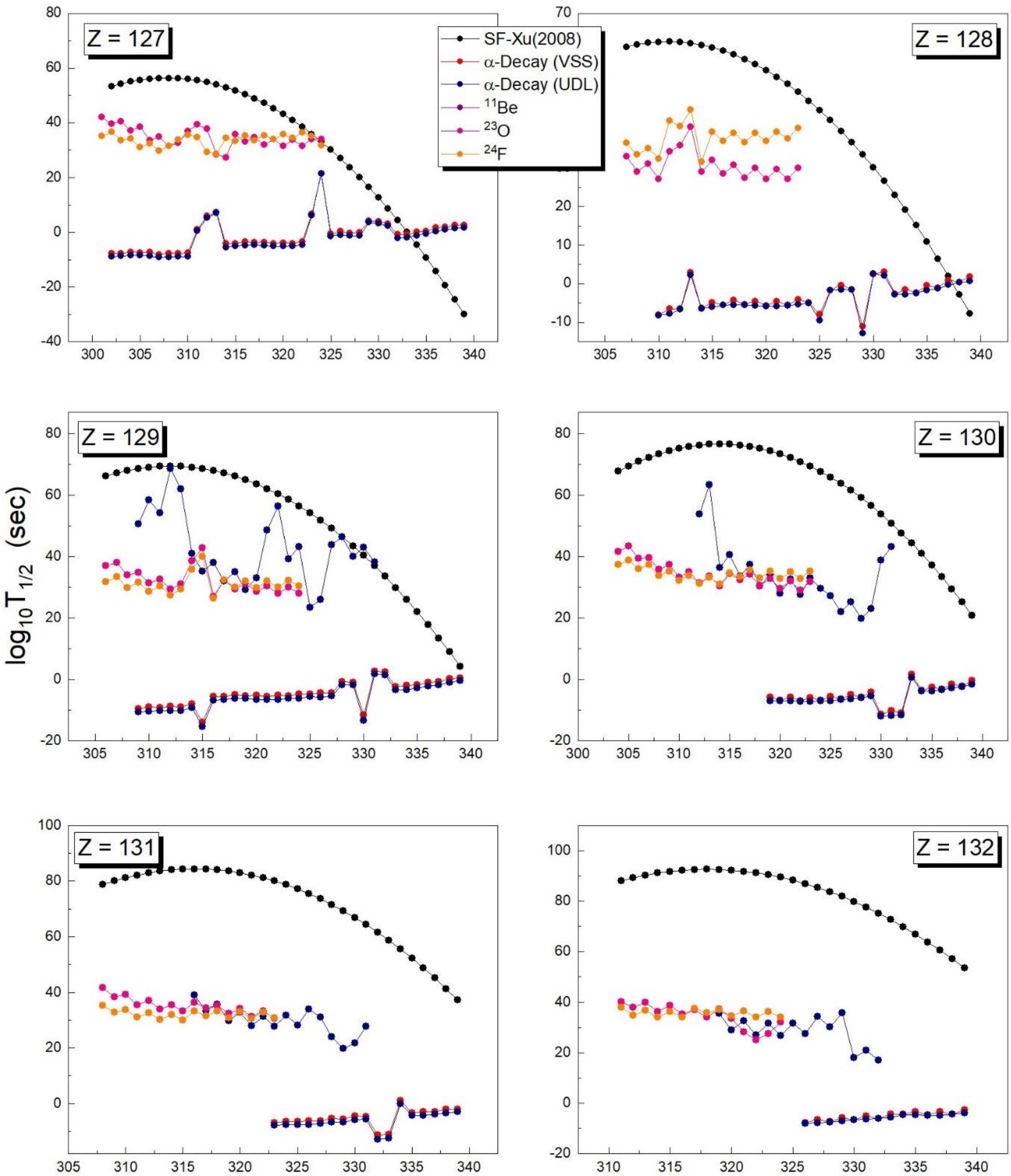


Fig. 3. Comparison of the half-life of spontaneous fission, alpha emission, and halo emission from $Z$ = 127 – 132 superheavy elements. (See color Figure on the journal website.)

Finally, Fig. 5 represents the universal curve between the logarithmic half-lives $\left(\log_{10} T_{1/2}\right)$ and the negative logarithm of penetrability ($-\ln P$) for the emission of $^{11}$Be and $^{23}$O and from $Z$ = 127 and 128 parent nuclei. The plots are linear with the same slope. From the other parents also, we got similar linear plots. Thus, from the linearity of the G-N plot and universal curve, it is clear that the CPPM can be used successfully for predicting the decay characteristics of various halo nuclei from superheavy elements. However, the predictions need experimental confirmation, and we hope in the near future our predictions will be verified with the availability of new experimental techniques.

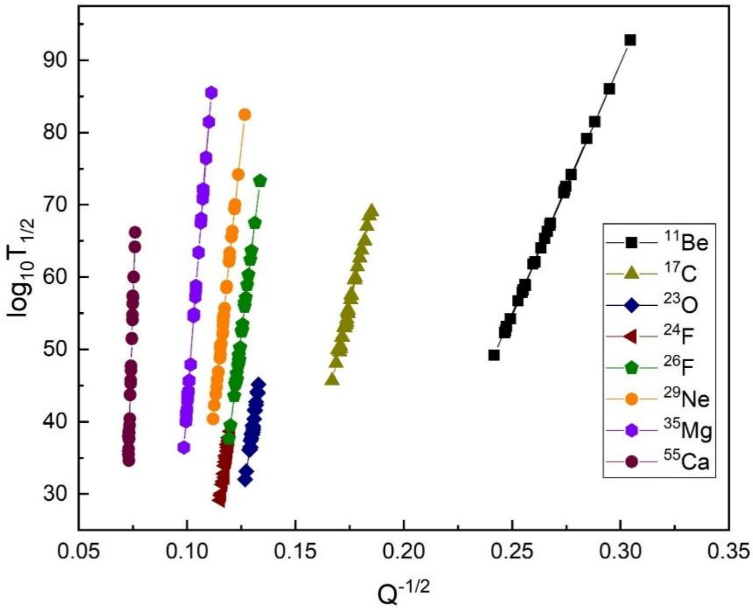


Fig. 4. G-N plot of $\log_{10}T_{1/2}$ versus $Q^{-1/2}$ for various neutron halos from superheavy nuclei with $Z$ = 127. (See color Figure on the journal website.)

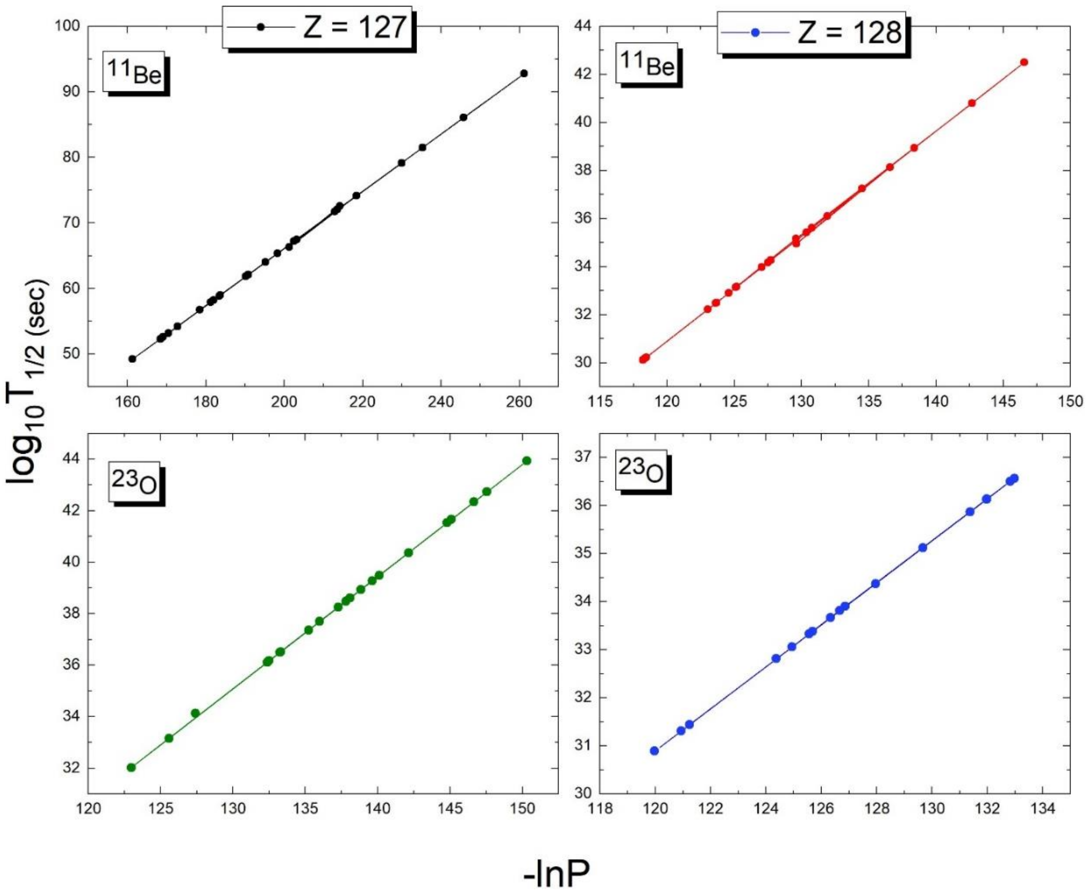


Fig. 5. The universal curve for calculated logarithmic half-lives ($\log_{10}T_{1/2}$) versus the negative logarithm of penetrability ($-\ln P$) for $^{11}$Be and $^{23}$O neutron halos from the superheavy nuclei with $Z$ = 127 and 128. (See color Figure on the journal website.)

We would like to point out that we have considered the halo nuclei as a normal cluster as well as a deformed nucleus with a rms radius. The low-density distribution is not considered in the calculations. This may result in a small amount of error, but it is within the admissible limit [66]. We hope that our study will provide insight into the synthesis of the superheavy elements through the fusion reactions.

## 4. Conclusion

The barrier penetrability, decay constant, and decay half-life of various 1-n and 2 -n halo nuclei from $Z = 127 - 132$ parents were calculated using the CPPM. For $^{11}$Be and $^{23}$O the decay half-lives are found to be within the experimental upper limit. It is observed that the decay half-life is decreased when the normal radius is replaced by the rms radius of the halo structure. The neutron shell closure at neutron numbers 190, 196, 198, 204, and 208 is evident from the plot $\log_{10} T_{1/2}$ versus the neutron number of daughter nuclei. The prominent peak in the plots at $N_p = 200$ indicates the exemptional stability of the parent nucleus and we predict 200 as a neutron magic number. For many of the parent nuclei, alpha decay is found to be the dominant decay mode. The linearity of G-N and universal plots corresponding to the emission of halo nuclei shows the validity of G-N law in the case of decay of halo nuclei from superheavy elements.

REFERENCES


1. P.G. Hansen, B. Jonson. The neutron halo of extremely neutron rich nuclei. Europh. Lett. 4(4) (1987) 409.
2. J. Al-Khalili. An introduction to halo nuclei. Lect. Notes Phys. 651 (2004) 77.
3. J. Al-Khalili, F. Nunes. Reaction models to probe the structure of light exotic nuclei. J. Phys. G 29(11) (2003) R89.
4. P.G. Hansen, A.S. Jensen, B. Jonson. Nuclear halos. Ann. Rev. Nucl. Part. Sci. 45 (1995) 591.
5. I. Tanihata et al. Measurement of interaction cross sections and nuclear radii in the light *p*-shell region. Phys. Rev. Lett. 55 (1985) 2676.
6. R. Kanungo et al. Proton distribution radii of $^{12\text{-}19}$C illuminate features of neutron halos. Phys. Rev. Lett. 117 (2016) 102501.
7. A. Estradé et al. Proton radii of $^{12\text{-}17}$B define a thick neutron surface in $^{17}$B. Phys. Rev. Lett. 113 (2014) 132501.
8. T. Bjerge, K. Broström. Ray spectrum of radio helium. Nature 138 (1936) 400.
9. S. Bottoni et al. Cluster-transfer reactions with radioactive beams: A spectroscopic tool for neutron-rich nuclei. Phys. Rev. C 92 (2015) 024322.
10. N. Kobayashi et al. One- and two-neutron removal reactions from the most neutron-rich carbon isotopes. Phys. Rev. C 86 (2012) 054604.
11. S.E.A. Orrigo, H. Lenske. Pairing resonances and continuum spectroscopy of $^{10}$Li. Phys. Lett. B 677 (2009) 214.
12. B. Jonson. Light dripline nuclei. Phys. Rep. 389 (2004) 1.
13. M.K. Sharma et al. Search for halo structure in $^{37}$Mg using the Glauber model and microscopic relativistic mean-field densities. Phys. Rev. C 93 (2016) 014322.
14. J. Al-Khalili, K. Arai. Excited state halos in $^{10}$Be. Phys. Rev. C 74 (2006) 034312.
15. H.Y. Zhang et al. Measurement of reaction cross section for proton-rich nuclei ($A < 30$) at intermediate energies. Nucl. Phys. A 707 (2002) 303.
16. I. Tanihata et al. Measurements of interaction cross sections and radii of He isotopes. Phys. Lett. B 160 (1985) 380.
17. A. Di Pietro et al. Experimental study of the collision $^{11}$Be + $^{64}$Zn around the Coulomb barrier. Phys. Rev. C 85 (2012) 054607.
18. S. Ahmad, A.A. Usmani, Z.A. Khan. Matter radii of light proton-rich and neutron-rich nuclear isotopes. Phys. Rev. C 96 (2017) 064602.
19. T. Nakamura et al. Halo structure of the island of inversion nucleus $^{31}$Ne. Phys. Rev. Lett. 103 (2009) 262501.
20. M. Takechi et al. Evidence of halo structure in $^{37}$Mg observed via reaction cross sections and intruder orbitals beyond the island of inversion. Phys. Rev. C 90 (2014) 061305(R).
21. M. Ismail, I.A.M. Abdul-Magead, Samar Gamal. Prediction of magic numbers of heavy and super heavy nuclei from the behavior of α-decay half-lives. IOSR J. Appl. Phys. 9(5) (2017) 64.
22. R.K. Gupta, S.K. Patra, W. Greiner. Structure of $^{294,302}$120 Nuclei Using the Relativistic Mean-Field Method. Mod. Phys. Lett. A 12 (1997) 1727.
23. M.V. Zhukov et al. Bound state properties of Borromean halo nuclei: $^{6}$He and $^{11}$Li. Phys. Rep. 231 (1993) 151.
24. D.J. Dean, M. Hjorth-Jensen. Pairing in nuclear systems: from neutron stars to finite nuclei. Rev. Mod. Phys. 75 (2003) 607.
25. A. Ono et al. Fragment formation studied with antisymmetrized version of molecular dynamics with two-nucleon collisions. Phys. Rev. Lett. 68(1992) 2898.
26. Y.K. Gambhir, P. Ring, A. Thimet. Relativistic mean field theory for finite nuclei. Ann. Phys. 198 (1990) 132.
27. S. Hofmann, G. Münzenberg. The discovery of the heaviest elements. Rev. Mod. Phys. 72 (2000) 733.
28. Yu. Oganessian. Heaviest nuclei from $^{48}$Ca-induced reactions. J. Phys. G 34(2007) R165.
29. Yu.Ts. Oganessian et al. Synthesis of the isotope $^{282}$113 in the $^{237}$Np + $^{48}$Ca fusion reaction. Phys. Rev. C 76 (2007) 011601(R).
30. V.Yu. Denisov, S. Hofmann. Formation of superheavy elements in cold fusion reactions. Phys. Rev. C 61 (2000) 034606.
31. S. Hofmann. Synthesis of superheavy elements using radioactive beams and targets. Prog. Part. Nucl. Phys. 46 (2001) 293.
32. J.H. Hamilton, S. Hofmann, Y.T. Oganessian. Search for super heavy nuclei. Annu. Rev. Nucl. Part. Sci. 63 (2013) 383.
33. Yu.Ts. Oganessian, V.K. Utyonkov. Superheavy nuclei from $^{48}$Ca-induced reactions. Nucl. Phys. A 944 (2015) 62.

34. N. Wang et al. Theoretical study of the synthesis of superheavy nuclei with Z = 119 and 120 in heavy-ion reactions with trans-uranium targets. Phys. Rev. C 85 (2012) 041601(R).
35. Yu.Ts. Oganessian et al. Synthesis of the isotopes of elements 118 and 116 in the $^{249}$Cf and $^{245}$Cm + $^{48}$Ca fusion reactions. Phys. Rev. C 74 (2006) 044602.
36. Z.-H. Liu, J.-D. Bao. Calculation of the evaporation residue cross sections for the synthesis of the superheavy element Z = 119 via the $^{50}$Ti + $^{249}$Bk hot fusion reaction. Phys. Rev. C 84 (2011) 031602(R).
37. K.P. Santhosh, V. Safoora. Synthesis of $^{292\text{-}303}$119 superheavy elements using Ca- and Ti-induced reactions. Phys. Rev. C 96 (2017) 034610.
38. F. Li. Predictions for the synthesis of superheavy elements Z = 119 and 120. Phys. Rev. C 98 (2018) 014618.
39. L. Zhu, W.-J. Xie, F.-S. Zhang. Production cross sections of superheavy elements Z = 119 and 120 in hot fusion reactions. Phys. Rev. C 89 (2014) 024615.
40. R.W. Lougheed et al. Search for superheavy elements using the $^{48}$Ca + $^{254}$Es$^{g}$ reaction. Phys. Rev. C 32 (1985) 1760.
41. S. Hofmann et al. Review of even element super-heavy nuclei and search for element 120. Eur. Phys. J. A 52 (2016) 180.
42. K.P. Santhosh, C. Nithya. Prediction on the modes of decay of even Z superheavy isotopes within the range $104 \le Z \le 136$. Atom. Data Nucl. Data Tabl. 119 (2018) 33.
43. K.P. Santhosh, B. Priyanka, C. Nithya. Feasibility of observing the α decay chains from isotopes of SHN with $Z = 128$, $Z = 126$, $Z = 124$ and $Z = 122$. Nucl. Phys. A 955 (2016) 156.
44. H.C. Manjunatha. Comparison of alpha decay with fission for isotopes of superheavy nuclei Z = 124. Int. J. Mod. Phys. E 25 (2016) 1650074.
45. H.C. Manjunatha. Alpha decay properties of superheavy nuclei Z = 126. Nucl. Phys. A 945 (2016) 42.
46. K.P. Anjali, K. Prathapan, R.K. Biju. Studies on the existence of various 1p, 2p halo isotopes via cluster decay of nuclei in superheavy region. Braz. J. Phys. 50(1) (2020) 71.
47. K.P. Anjali, K. Prathapan, R.K. Biju. A study on the emission of 1, 2 proton halo nuclei from parent with $Z = 121 - 128$ in the superheavy nuclei via cluster radioactivity. Braz. J. Phys. 50 (2020) 298.
48. K.P. Santhosh, R.K. Biju, S. Sahadevan. Cluster formation probability in the trans-tin and trans-lead nuclei. Nucl. Phys. A 838 (2010) 38.
49. Y.-J. Shi, W.J. Swiatecki. Theoretical estimates of the rates of radioactive decay of radium isotopes by $^{14}$C emission. Phys. Rev. Lett. 54 (1985) 300.
50. J. Blocki et al. Proximity forces. Ann. Phys. 105 (1977) 427.
51. J. Blocki, W.J. Swiatecki. A generalization of the proximity force theorem. Ann. Phys. 132 (1981) 53.
52. D.N. Poenaru et al. Atomic nuclei decay modes by spontaneous emission of heavy ions. Phys. Rev. C 32 (1985) 572.
53. K.P. Santhosh, I. Sukumaran, B. Priyanka. Theoretical studies on the alpha decay of $^{178\text{-}220}$Pb isotopes. Nucl. Phys. A 935 (2015) 28.
54. K.P. Santhosh, I. Sukumaran. Decay of Z = 82 – 102 heavy nuclei via emission of one-proton and two-proton halo nuclei. Pramana J. Phys. 92 (2019) 6.
55. K.P. Santhosh, C. Nithya. Predictions on the modes of decay of odd Z superheavy isotopes within the range $105 < Z < 135$. Atom. Data Nucl. Data Tabl. 121-122 (2018) 216.
56. K.P. Santhosh, I. Sukumaran. Decay of heavy particles from Z = 125 superheavy nuclei in the region $A = 295 - 325$ using different versions of proximity potential. Int. J. Mod. Phys. E 26(03) (2017) 1750003.
57. K.P. Santhosh, B. Priyanka. Probable cluster decays from $^{270\text{-}318}$118 superheavy nuclei. Int. J. Mod. Phys. E 23(10) (2014) 1450059.
58. K.P. Santhosh, R.K. Biju. Alpha decay, cluster decay and spontaneous fission in $^{294\text{-}326}$122 isotopes. J. Phys. G 36(1) (2009) 015107.
59. D.N. Poenaru, I.-H. Plonski, W. Greiner. α-decay half-lives of superheavy nuclei. Phys. Rev. C 74 (2006) 014312.
60. G. Royer, H.F. Zhang. Recent α decay half-lives and analytic expression predictions including superheavy nuclei. Phys. Rev. C 77 (2008) 037602.
61. V.E. Viola, G.T. Seaborg. Nuclear systematics of the heavy elements – II Lifetimes for alpha, beta and spontaneous fission decay. J. Inorg. Nucl. Chem. 28 (1966) 741.
62. A. Zdeb, M. Warda, C.M. Petrache. Proton emission half-lives within a Gamow-like model. Eur. Phys. J. A 52 (2016) 323.
63. Y. Hatsukawa, H. Nakahara, D.C. Hoffman. Systematics of alpha decay half-lives. Phys. Rev. C 42 (1990) 674.
64. K.P. Anjali, K. Prathapan, R.K. Biju. Studies on the emission of various exotic fragments from super-heavy nuclei via cluster decay process. Nucl. Phys. A 993 (2020) 121644.
65. K. Prathapan, K.P. Anjali, R.K. Biju. Existence of $^{15\text{-}21}$N, $^{17\text{-}23}$O, and $^{19\text{-}25}$F neutron halo nuclei via cluster decay process in the superheavy region. Braz. J. Phys. 49(5) (2019) 752.
66. K.P. Santhosh, I. Sukumaran. A systematic study on 1neutron and 2neutron halo nuclei using coulomb and nuclear proximity potential. Braz. J. Phys. 48 (2018) 497.
67. V.Y. Denisov, H. Ikezoe. α-nucleus potential for α-decay and sub-barrier fusion. Phys. Rev. C 72 (2005) 064613.
68. K.-N. Huang et al. Neutral-atom electron binding energies from relaxed-orbital relativistic Hartree-Fock-Slater calculations $2 \le Z \le 106$. Atom. Data Nucl. Data Tabl. 18 (1976) 243.
69. H. Koura. Nuclidic mass formula on a spherical basis with an improved even-odd term. Prog. Theor. Phys. 113 (2005) 305.
70. P. Möller et al. Nuclear ground-state masses and deformations: FRDM (2012). Atom. Data Nucl. Data Tabl. 109-110 (2016) 1.

71. A. Ozawa, T. Suzuki, I. Tanihata. Nuclear size and related topics. Nucl. Phys. A 693 (2001) 32.
72. M.Y. Ismail et al. Effect of choosing the $Q_\alpha$-values and daughter density distributions on the magic numbers predicted by α decays. Ann. Phys. 406 (2019) 1.
73. C. Xu, Z. Ren, Y. Guo. Competition between α decay and spontaneous fission for heavy and superheavy nuclei. Phys. Rev. C 78 (2008) 044329.
74. A. Sobiczewski, Z. Patyk, S. Ćwiok. Deformed superheavy nuclei. Phys. Lett. B 224 (1989) 1.
75. C. Qi et al. Microscopic mechanism of charged-particle radioactivity and generalization of the Geiger-Nuttall law. Phys. Rev. C 80 (2009) 044326.
76. I. Muntian, Z. Patyk, A. Sobiczewski. Calculated masses of heaviest nuclei. Phys. Atom. Nucl. 66 (2003) 1015.
77. S. Hofmann. Search for isotopes of element 120 on the island of SHN. In: International Symposium on Exotic Nuclei. EXON-2014. Kaliningrad, Russia, 8 - 13 September 2014. Yu.E. Penionzhkevich, Yu.G. Sobolev (Eds.) (World Scientific Publishing Co. Pte. Ltd., 2015) p. 213.
78. S. Hofmann. Overview and perspectives of SHE research at GSI SHIP. In: W. Greiner (Ed.). Exciting Interdisciplinary Physics. FIAS Interdisciplinary Science Series (Switzerland, Springer Int. Publ., 2013) p. 23.
79. S. Heinz. Multinucleon transfer reactions – a pathway to new heavy and superheavy nuclei? J. Phys.: Conf. Ser. 1014 (2018) 012005.
80. S. Hofmann. Super-heavy nuclei. J. Phys. G 42 (2015) 114001.
81. J. Khuyagbaatar et al. Fission in the landscape of heaviest elements: Some recent examples. EPJ Web Conf. 131 (2016) 03003.
82. T. Niwase et al. Development of an “α-TOF” detector for correlated measurement of atomic masses and decay properties. Nucl. Instrum. Meth. A 953 (2020) 163198.
83. S. Ishizawa et al. Improvement of the detection efficiency of a time-of-flight detector for superheavy element search. Nucl. Instrum. Meth. A 960 (2020) 163614.
84. H. Geiger, J.M. Nuttall. The ranges of the α particles from various radioactive substances and a relation between range and period of transformation. Philos. Mag. 22 (1911) 613.
85. C. Qi, R.J. Liotta, R. Wyss. Generalization of the Geiger-Nuttall law and alpha clustering in heavy nuclei. J. Phys.: Conf. Ser. 381 (2012) 012131.
86. S. Kumar, R.K. Gupta. Measurable decay modes of barium isotopes via exotic cluster emissions. Phys. Rev. C 49 (1994) 1922.
87. S. Kumar, D. Bir, R.K. Gupta. $^{100}$daughter α-nuclei cluster decays of some neutron-deficient Xe to Gd parents: Sn radioactivity. Phys. Rev. C 51 (1995) 1762.
88. K.P. Santhosh, A. Joseph. Exotic decay in Ba isotopes via $^{12}$C emission. Pramana J. Phys. 55 (2000) 375.
89. K.P. Santhosh, A. Joseph. Exotic decay in cerium isotopes. Pramana J. Phys. 58 (2002) 611.



**К. Пратхапан[1], М. К. Прітхі Раджан[2], Р. К. Біжу[1,3,*]**

*[1] Факультет фізики, Державний коледж Бреннен, Талассері, Індія*
*[2] Факультет фізики, Коледж Пайянур, Пайянур, Індія*
*[3] Факультет фізики, Коледж Пажасі Раджа НСС, Маттанур, Індія*

*Відповідальний автор: bijurkn@gmail.com


## ДОСЛІДЖЕННЯ РОЗПАДУ НАДВАЖКИХ ЯДЕР З Z = 127 – 132 З ВИПРОМІНЮВАННЯМ 1-N І 2-N ГАЛО-ЯДЕР


Проникність бар’єрів, константа розпаду та період напіврозпаду для 1-n гало-ядер $^{11}$Be, $^{15,17,19}$C, $^{22}$N, $^{23}$O, $^{24,26}$F, $^{29,31}$Ne, $^{34,37}$Na, $^{35,37}$Mg і $^{55}$Ca; і 2-n гало ядер $^{22}$C, $^{27,29}$F, $^{34}$Ne, $^{36}$Na і $^{46}$P і материнських ядер з Z = 127 – 132 були розраховані в рамках моделі з Кулонівським потенціалом та потенціалом близькості при отриманні значень Q в краплинній моделі. Було проведено порівняння між періодами напіврозпаду при розгляді гало-кандидатів як нормальних кластерів і як деформованих утворень із відповідним середньоквадратичним радіусом. Закриття нейтронної оболонки на значеннях 190, 196, 198, 200, 204 і 208 було визначено з графіка періодів напіврозпаду залежно від числа нейтронів дочірніх ядер ($N_P$). Розрахунки періоду напіврозпаду для альфа-розпаду і спонтанного розпаду показали, що більшість материнських ядер розпадається більш імовірно через альфа-випромінювання. Графіки Гейгера - Неттолла $\log_{10}T_{1/2}$ залежно від $Q^{-1/2}$ та універсальні графіки $\log_{10}T_{1/2}$ залежно від $-\ln P$ для випромінювання всіх 1-n і 2-n гало-ядер з материнських ядер, що розглядається тут, є лінійними, що показує справедливість закону Гейгера - Неттола для емісії гало-ядер з надважких елементів.



*Ключові слова*: кластерна радіоактивність, гало-ядра, надважкі елементи.

Надійшла/Received 28.06.2023